PHYSICAL REVIEW B **84**, 184524 (2011)

Volovik effect in a highly anisotropic multiband superconductor: Experiment and theory

Y. Wang, J. S. Kim, G. R. Stewart, and P. J. Hirschfeld
Department of Physics, University of Florida, Gainesville, Florida 32611, USA

S. Graser
Center for Electronic Correlations and Magnetism, Institute of Physics, University of Augsburg, D-86135 Augsburg, Germany

S. Kasahara and T. Terashima
Research Center for Low Temperature and Materials Sciences, Kyoto University, Kyoto 606-8501, Japan

Y. Matsuda and T. Shibauchi
Department of Physics, Kyoto University, Sakyo-ku, Kyoto 606-8502, Japan

I. Vekhter
Department of Physics and Astronomy, Louisiana State University, Baton Rouge, Louisiana 70803, USA
(Received 1 September 2011; revised manuscript received 1 November 2011; published 17 November 2011)

We present measurements of the specific heat coefficient γ ($\equiv C/T$) in the low-temperature limit as a function of an applied magnetic field for the Fe-based superconductor $BaFe_2(As_{0.7}P_{0.3})_2$. We find both a linear regime at higher fields and a limiting square root H behavior at very low fields. The crossover from a Volovik-like $\sqrt{H}$ to a linear field dependence can be understood from a multiband calculation in the quasiclassical approximation assuming gaps with different momentum dependence on the hole- and electronlike Fermi surface sheets.

DOI: 10.1103/PhysRevB.84.184524 PACS number(s): 74.70.Xa, 74.20.Rp, 74.25.Bt

I. INTRODUCTION

The symmetry and detailed structure of the gap function in the recently discovered iron pnictide[1] and chalcogenide[2] high-temperature superconductors are still under discussion. Across an increasingly numerous set of materials families, as well as within each family where superconductivity can be tuned by doping or pressure, experimental indications are that there is no universal gap structure.[3,4] Instead, the superconducting gap appears to be remarkably sensitive to details of the normal-state properties. This "intrinsic sensitivity"[5] may be due to the unusual Fermi surface topology, consisting of small hole and electron pockets, and to the probable A_{1g} symmetry of the superconducting gap, which allows a continuous deformation of the order parameter structure from a fully gapped system to one with nodes (for a review, see, e.g., Ref. 6). It is important to keep in mind, though, that another possibility to account for the observed variability is that different experiments on the same material may probe selectively different Fermi surface regions and hence different gaps within the system.

The Ba-122 family of materials has been intensively studied because large high-quality single crystals are relatively easy to produce.[4,7] Within this family, the isovalently substituted system $BaFe_2(As_{1-x}P_x)_2$ with a maximum T_c of 31 K is particularly intriguing because it exhibits a phase diagram and transport properties remarkably similar to those of the heterovalently doped system $Ba(Fe_{1-x}Co_x)_2As_2$ and displays many signatures of apparent quantum critical behavior at optimal doping.[7–9] In the superconducting state, penetration depth,[10] nuclear magnetic resonance (NMR) spin-lattice relaxation,[11] and the temperature dependence[10] and angular field variation[12] of the thermal conductivity show clear indications of nodal behavior. Surprisingly, a linear field dependence of the specific heat Sommerfeld coefficient γ was measured[13] on optimally doped samples from the same batch. Such behavior is expected for a fully gapped single-band superconductor since the fermionic excitations from the normal cores of vortices provide the only contribution to γ at low T, and the number of these vortices scales linearly with the field H. It was argued in Ref. 13 that the specific heat measurement might be consistent with the other experiments suggesting nodes if the heavy-hole sheets in the material were fully gapped while the gaps on the lighter electron sheets were nodal. In such a case the $\gamma \sim \sqrt{H}$ behavior would be difficult to observe in experiment.

In this paper, we report new experimental data on the magnetic field dependence of the specific heat of optimally doped $BaFe_2(As_{1-x}P_x)_2$ samples. We have extended our previous measurements to 15 T to higher fields up to 35 T [$\approx \frac{2}{3}H_{c2}(0)$], where we find a continuation of the linear behavior reported earlier. However, more precise measurements at low fields have revealed the presence of a Volovik-like $\sqrt{H}$ term which persists roughly over a range of 4 T, crossing over to a linear behavior above this scale.[14] The observation of this term, consistent with nodes in the superconducting gap, therefore supports claims made in earlier work,[10–12] without the need to assume an extremely large mass on the hole pockets.

Theoretical estimates using the Doppler-shift method for isotropic gaps given in Ref. 15 were oversimplified, but did show the need for a more thorough analysis of anisotropic multiband systems and stimulated further experimental work, both of which we report here. The theoretical difficulties can be seen easily by considering a simple two-band model with two distinct gaps Δ_1 and Δ_2, where we assume for the moment that $\Delta_2 > \Delta_1$. If the two bands are uncoupled, the two gaps correspond to two independent coherence lengths $\xi_i \simeq v_{F,i}/(\pi\Delta_i)$, where $i = 1,2$, and two independent "upper

critical fields" $H_{c2,i}$. Vortex core states of the large gap Δ_2 are confined to cores of radius $\sim\xi_2$. For fields in the range $H_{c2,1} \lesssim H \lesssim H_{c2,2}$, the vortex cores of the small gap will overlap, while the large-gap cores will still be well separated. Note that if Δ_1 is very small (these considerations also describe crudely nodal gaps), this field range can be wide and can extend to quite low fields. On the other hand, methods of studying quasiparticle properties in superconductors are typically adapted to calculations near H_{c1} or H_{c2}, i.e., in the limit of widely separated or nearly overlapping vortices. The current problem apparently contains elements of both situations. In the absence of interband coupling, of course, one can use different methods, corresponding to the appropriate field regimes, for the distinct bands. For coupled Fermi surfaces, however, such an approach is not viable. In the immediate vicinity of the transition, where the Ginzburg-Landau expansion is valid, there is a single length scale controlling the vortex structure.[16] At low temperatures, where the measurements are carried out, however, the distinct length scales likely survive, although they are modified by the strength of the interband coupling (see below). Possible anisotropy of the gap on one or more Fermi surface sheets complicates the picture even further. We show here that judicious use of the quasiclassical approximation even with simplifying assumptions about the vortex structure can provide a general framework for the description of this problem and a semiquantitative understanding of the new data on the $BaFe_2(As_{1-x}P_x)_2$ system. We compare our results with those obtained by Doppler-shift methods and show that if properly implemented this method also gives reasonable qualitative results in the low-field range.

This joint theory-experiment paper is organized as follows. We first present our experimental results on the $BaFe_2(As_{1-x}P_x)_2$ system in Sec. II and compare to our previous results, as well as to data by other groups on the related heterovalently doped Ba-122 materials. In Sec. III, we discuss the two-band quasiclassical model we use to study the system, and in Sec. IV we give our results. Finally, in Sec. V we present our conclusions.

II. EXPERIMENT

Tiny platelet crystals of $BaFe_2(As_{0.7}P_{0.3})_2$ were prepared as described in Ref. 7. Subsequent measurements on crystals extracted from various positions in the crucible using x-ray diffraction and energy dispersion x-ray analysis give a phosphorus concentration of $(32.9 \pm 0.4)\%$. A further test of the homogeneity of the crystals from a given growth batch is the measurement of the susceptibility at the superconducting transition as shown in Fig. 1 of Ref. 13. Here, for a collage of ~150 mg of these crystals a rather narrow transition was observed. A collage of 18 mg of these microcrystals was then mounted on a sapphire disk using GE7031 varnish. Approximately 75% of the crystals had the magnetic field perpendicular to the a-b plane (the plane of the crystals), whereas the remaining crystals were randomly oriented. The sapphire disk was mounted in our time constant method calorimeter,[17] and the specific heat from 0.4 to 7 K in fields from 0 to 35 T was measured. Additionally, the specific heat of a standard (high-purity Au) was measured in fields up to 14 T. Results on the standard (not shown) indicate agreement with published values to within $\pm 3\%$ in all fields.

A. Results and discussion

The specific heat coefficient $\gamma \equiv C/T$ of $BaFe_2(As_{0.7}P_{0.3})_2$ for $0 \leqslant H \leqslant 35$ T is shown by the open triangles in Fig. 1. There is a small low-temperature anomaly in the specific heat data below about 1.4 K (discussed in detail in Ref. 13). Such anomalies have been observed in other FePn samples,[18] and in some cases, e.g., in $BaFe_{2-x}Co_xAs_2$, they show a rather strong magnetic field dependence.[18] However, as discussed in our previous report[13] of the data up to 15 T, the anomaly in $BaFe_2(As_{0.7}P_{0.3})_2$ is approximately field independent. Note that the small anomaly in the specific heat appears to vanish above 1.4 K, i.e., does not affect the estimate for γ shown in Figs. 1 and 2 using data from 1.5 K and above.

In order to have a closer look at the low-field dependence of the specific heat, these data are shown on an expanded scale in Fig. 2. In our analysis below, we focus on the asymptotic $T \to 0$ behavior since it is directly related to the density of states at the Fermi level, which is easy to calculate reliably, and since it gives essentially the same field dependence as the nonzero-T data.

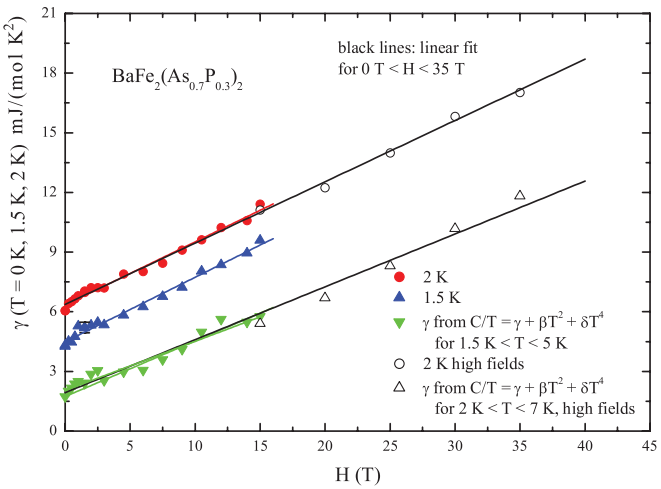

FIG. 1. (Color online) The original specific heat data (Ref. 13) on $BaFe_2(As_{0.7}P_{0.3})_2$ as a function of field up to 15 T (solid symbols) with data from present work between 15 and 35 T (open symbols). Note the agreement between the linear, $C/T \propto H$, extrapolation of the 15 T [colored lines (Ref. 13)] and 35 T (black lines, present work) results. We extract γ from the data using two (equivalent) methods: (a) by making an extrapolation $C/T = \gamma + \beta T^2 + \delta T^4$ from 2 K and above or (b) by taking the smoothed value of C/T at 1.5 and 2 K found by fitting approximately ten data points around these temperatures to obtain C/T (1.5 K) and C/T (2 K) with decreased scatter. The temperature restriction eliminates both the influence of the anomaly and the field-induced nuclear contribution (see text), negligible for $H \leqslant 4$ T above 1 K. The absolute accuracy of these data is $\pm 5\%$ (error bars are not shown at low fields since they are approximately the same size as a data point), while the precision of the data is approximately $\pm 2\%$. In addition, additional data with finer gradations in the measured fields up to 4 T were taken to explore the low-field nonlinear behavior. These data are shown on an expanded scale in Fig. 2.

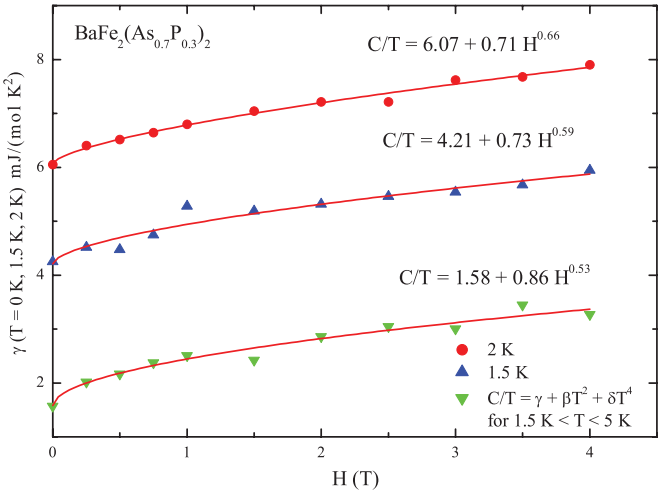

FIG. 2. (Color online) Low-field γ data up to 4 T from Fig. 1 on an expanded scale for $T = 2$ K (red dots) and 1.5 K (blue up triangles). Green down triangles show asymptotic $\lim_{T\to 0} C/T$ determined over the range $1.5 < T < 5$ K. The fitting functions of the data are labeled beside the curves. Best power-law fits to field dependence are shown in each case.

III. MODEL

A. Quasiclassical approximation

The quasiclassical (Eilenberger) approximation[19–21] is a powerful tool to describe the electronic properties of the superconducting state on scales large compared to the lattice spacing, provided the condition $k_F\xi \gg 1$ is satisfied. Here k_F is the Fermi momentum and ξ the coherence length. Since in this limit we can think of quasiparticles as propagating coherently along a well-defined trajectory in real space, this method is particularly well suited to address inhomogeneous situations, such as the vortex state of type-II superconductors (SCs). An alternative and frequently used approach to the vortex state is to take into account the (classical) shift of the quasiparticle energy due to the local supercurrent flow. This approximation, often referred to as the Doppler-shift approach, is valid for nodal SCs with considerable weight of extended quasiparticle excitations ouside the vortex cores. Using this method, Volovik showed that for superconductors with line nodes these extended quasiparticle excitations lead to a nonlinear magnetic field dependence of the spatially averaged residual density of states $N(\omega = 0, H) \propto N_0\sqrt{H/H_{c2}}$, the result known as the Volovik effect.[22] This behavior was first confirmed by measurements of the specific heat[23,24] and by subsequent calculations within the quasiclassical approximation for both a single vortex in a d-wave SC (Refs. 25 and 26) and a vortex lattice.[27,28] Both quasiclassical and Doppler-shift methods fail at the lowest temperatures due to quantum effects,[29] but in known systems with $T_c \ll E_F$ these effects are negligible in practice. Both methods have successfully explained at a semiquantitative level the magnetic field dependence of the specific heat and thermal conductivity in a wide variety of unconventional superconductors.[30] It was also shown that the accurately calculated quasiparticle excitation spectrum is consistent with scanning tunneling microscopy studies of the electronic structure around a vortex core.[27]

Many experimental techniques which are sensitive to the low-energy density of states, such as measurements of thermal conductivity, specific heat, and NMR relaxation rate, can be used to draw conclusions about the possible existence and the momentum dependence of quasiparticle excitations in the bulk of iron-based superconductors (FeSCs) and thus about the structure of the superconducting gap and the distribution of gap nodes. The low-T limit of the Sommerfeld coefficient in an applied magnetic field, $\gamma(H)$, is directly proportional to the spatially averaged local density of states (LDOS) at the Fermi level. The Doppler-shift method has been used to calculate the LDOS for a two-band SC with two isotropic gaps of unequal size $\Delta_S \neq \Delta_L$ and to give an interpretation of the experimental data available at that time.[15] However, the Doppler-shift approach cannot account properly for the contributions from the states in the vortex core that have a very large weight in the net DOS and hence gives a quantitatively and sometimes qualitatively inaccurate description of the electronic structure of the vortex. For example, in a simple d-wave superconductor, the spatial tails of the low-energy density of states around the vortex are aligned in the wrong directions.[31] To obtain a quantitative fit to the specific heat data presented in the previous section and to allow for a more decisive conclusion about the gap structure of $BaFe_2(As_{0.7}P_{0.3})_2$, we will therefore use the quasiclassical approximation, which we will briefly review in the following paragraphs.

In the quasiclassical method, the Gorkov Green's functions are integrated with respect to the quasiparticle energy measured from the Fermi level. The normal and anomalous components $g(\mathbf{r},\theta,i\omega_n)$ and $f(\mathbf{r},\theta,i\omega_n)$ of the resulting propagator $\hat{g}$ obey the coupled Eilenberger equations

$$\left[2\left(i\omega_n + \frac{e}{c}\mathbf{v}_F\cdot\mathbf{A}(\mathbf{r})\right) + i\hbar\mathbf{v}_F\cdot\nabla\right] f(\mathbf{r},\theta,i\omega_n) = 2ig(\mathbf{r},\theta,i\omega_n)\Delta(\mathbf{r},\theta), \tag{1a}$$

$$\left[2\left(i\omega_n + \frac{e}{c}\mathbf{v}_F\cdot\mathbf{A}(\mathbf{r})\right) - i\hbar\mathbf{v}_F\cdot\nabla\right] \bar{f}(\mathbf{r},\theta,i\omega_n) = 2ig(\mathbf{r},\theta,i\omega_n)\Delta^*(\mathbf{r},\theta), \tag{1b}$$

that have to be complemented by the normalization condition

$$\hat{g}^2 \equiv \begin{pmatrix} g & f \\ \bar{f} & -g \end{pmatrix}^2 = \hat{1}. \tag{2}$$

Here $\Delta(\mathbf{r},\theta)$ is the order parameter, $\mathbf{A}(\mathbf{r})$ the vector potential, $\mathbf{v}_F$ the Fermi velocity at the location at the Fermi surface labeled by θ, and $\omega_n = (2n+1)\pi k_B T$ the fermionic Matsubara frequencies. For two-dimensional cylindrical Fermi surfaces such as those considered below, $\mathbf{v}_F = v_F\hat{\mathbf{k}}$ where $\hat{\mathbf{k}} = (\cos\theta, \sin\theta)$ and θ is the angle measured from the [100] direction. In that case it is natural to write the position vector in cylindrical coordinates, $\mathbf{r} = (\rho,\phi,z)$, where ϕ is the winding angle around the vortex in real space.

Making use of the symmetries[32] of the quasiclassical propagator,[33]

$$\bar{f}(\mathbf{r},\mathbf{k}_F,i\omega_n) = f^*(\mathbf{r},\mathbf{k}_F,-i\omega_n), \tag{3a}$$

$$f(\mathbf{r},-\mathbf{k}_F,-i\omega_n) = f(\mathbf{r},\mathbf{k}_F,i\omega_n), \tag{3b}$$

$$g(\mathbf{r},\mathbf{k}_F,i\omega_n) = g^*(\mathbf{r},\mathbf{k}_F,-i\omega_n), \tag{3c}$$

the diagonal part of the normalization condition (2) can be written in a more explicit form as

$$[g(\mathbf{r},\theta,i\omega_n)]^2 + f(\mathbf{r},\theta,i\omega_n)f^*(\mathbf{r},\theta+\pi,i\omega_n) = 1. \quad (4)$$

Instead of solving the complicated coupled Eilenberger equations everywhere in space, we follow Refs. 26 and 32 and parametrize the quasiclassical propagator along real space trajectories $\mathbf{r}(x) = \mathbf{r}_0 + x\hat{\mathbf{v}}_F$ by a set of scalar amplitudes $a(x)$ and $b(x)$,

$$\hat{g}(\mathbf{r}(x)) = \frac{1}{1+a(x)b(x)}\begin{pmatrix} 1-a(x)b(x) & 2a(x) \\ 2b(x) & -1+a(x)b(x) \end{pmatrix}. \quad (5)$$

These amplitudes obey numerically stable Riccati equations,

$$v_F\partial_x a(x) + [2\tilde{\omega}_n + \Delta^*(x)a(x)]a(x) - \Delta(x) = 0, \quad (6a)$$

$$v_F\partial_x b(x) - [2\tilde{\omega}_n + \Delta(x)b(x)]b(x) + \Delta^*(x) = 0. \quad (6b)$$

For the single-vortex problem the spatial dependence vanishes far away from the vortex core, and hence we have the initial conditions

$$a(-\infty) = \frac{\Delta(-\infty)}{\omega_n + \sqrt{\omega_n^2 + |\Delta(-\infty)|^2}}, \quad (7a)$$

$$b(+\infty) = \frac{\Delta^*(+\infty)}{\omega_n + \sqrt{\omega_n^2 + |\Delta(+\infty)|^2}}. \quad (7b)$$

Here we have set $\hbar = 1$ and we have introduced the modified Matsubara frequencies $i\tilde{\omega}_n(x) = i\omega_n + (e/c)\mathbf{v}_F \cdot \mathbf{A}(x)$. Since the modification of the Matsubara frequencies due to the external field is of the order of $1/\kappa^2$ where $\kappa = \lambda_L/\xi$ is the ratio of the London penetration depth and the coherence length, the term proportional to $\mathbf{A}(x)$ in Eq. (6) can be neglected for strong type-II superconductors.

After an analytic continuation of the Matsubara frequencies to the real axis, $i\omega_n \to \omega + i\delta$, the local density of states can be calculated as the Fermi surface average of the quasiclassical propagator,

$$N(\mathbf{r}) = N_0 \int_0^{2\pi} \frac{d\theta}{2\pi} \mathrm{Re}\left(\frac{1-ab}{1+ab}\right)_{i\omega_n\to\omega+i\delta}, \quad (8)$$

where N_0 is the normal density of states at the Fermi energy. To obtain stable numerical solutions we use a small imaginary part $\delta = 0.02T_c$ in the analytical continuation, where T_c is the critical temperature of the superconductor.

B. Two-band model

The Fermi surface of the optimally doped $BaFe_2(As_{0.7}P_{0.3})_2$ consists of multiple Fermi surface sheets. Density functional theory (DFT) calculations showed that there are three concentric hole cylinders in the center of the Brillouin zone (Γ point) and two electron pockets at the zone corner (X point).[34] Laser angle-resolved photoemission spectroscopy (ARPES) measurements[35] found a superconducting order parameter that is fully gapped with comparably sized gaps on each hole pocket of the order of $\Delta_h/k_BT_c \sim 1.7$. Taking into account the results from thermal conductivity[10,12] and NMR measurements[11] as well as the measurements of the specific heat coefficient in low fields presented above, which all consistently report evidence for low-energy quasiparticles, this ARPES result implies a nodal gap on the electron pockets.

For numerical convenience we adopt below a two-band model, distinguishing only between electron and hole pockets. Inclusion of all Fermi surface sheets then enters only as a weighting factor for the electron and hole pocket contributions, as we discuss in the following section. We take the gaps on the electron and hole pockets in the form $\Delta_{1,2}(\theta) = \Delta_0^{e,h}\Phi_{1,2}(\theta)$, where the angle θ parametrizes the appropriate Fermi surface, assumed to be cylindrical. We assume an anisotropic gap on the electron pocket,[36] $\Phi_1(\theta) = (1 + r\cos 2\theta)/\sqrt{1+r^2/2}$, and an isotropic gap around the hole Fermi surface, $\Phi_2(\theta) = 1$. If the anisotropy factor $r > 1$, the superconducting gap in the electron band, $\Delta_1(\theta)$, has accidental nodes; if $r = 0$, $\Delta_1(\theta)$ is isotropic like $\Delta_2(\theta)$.

First we assume $\Delta_0^e = \Delta_0^h$, as is often found by ARPES (at this writing there are to our knowledge no ARPES results on this material which resolve the gap on the electron pocket). Since we consider well-separated electron and hole bands, we can solve the Riccati equations (6) for the two propagators separately, and the only coupling of the pockets is via the self-consistency equations on the order parameter (see below). With this in mind we normalize the energy and length for the electron and hole bands by the gap amplitudes Δ_0^e and Δ_0^h and the coherence lengths $\xi_0^e = v_F^e/\Delta_0^e$ and $\xi_0^h = v_F^h/\Delta_0^h$, respectively. Fermi velocities therefore appear as an input. DFT calculations for a comparable Ba-122 system[37] give $v_F^h = 1.979 \times 10^5$ m/s and $v_F^e = 3.023 \times 10^5$ m/s, i.e., $v_F^h/v_F^e = \xi_0^h/\xi_0^e = 0.65$. In our analysis we keep this ratio but reduce the value of both Fermi velocities by a factor of 5 to approximately account for the mass renormalization of this system near optimal doping.[9,38] This reduction also gives a roughly correct value of the c-axis upper critical field $H_{c2} \sim 50$ T. In the limit of negligible coupling between the bands, the upper critical field is determined by the overlap of the vortices with smallest core size,

$$\frac{R}{\min\{\xi_0^e,\xi_0^h\}} = \frac{R}{\xi_0^h} = \sqrt{\frac{H_{c2}}{H}}. \quad (9)$$

Below we solve the Eilenberger equations and determine the density of states for an isolated vortex and for each band separately. In a two-band system the spatial profile of the quasiparticle states on the electron and hole bands is controlled by the respective coherence lengths, and therefore spatial averaging weights the contributions of the bands differently compared to the DOS of a system with a single or two equal coherence lengths. This is the most significant difference compared to a single-band model.

The superconducting order parameters in the two bands are related by the interband component of the pairing interaction. We consider a general coupling matrix in the factorized form, $\lambda_{\nu\mu}(\theta,\theta') = \lambda_{\nu\mu}\Phi_\nu(\theta)\Phi_\mu(\theta')$, where $\mu,\nu = 1,2$ and $\lambda_{\nu\mu} \equiv V_{\nu\mu}N_\mu$. Here $V_{11} = V_e$ and $V_{22} = V_h$ are the intraband pairing interactions in the electron and the hole band, respectively, while $V_{12} = V_{eh}$ is the interband interaction. N_μ is the normal

density of states at the Fermi level. Then the gap equation for an inhomogeneous superconductor is

$$\Delta_\nu(\mathbf{r}) = 2\pi T \sum_{\mu=1,2} \lambda_{\nu\mu} \sum_{\omega_n>0}^{\omega_c} \langle \Phi_\mu(\theta) f_\mu(\mathbf{r},\theta,i\omega_n)\rangle_\theta. \quad (10)$$

Here $\Delta_\nu(\mathbf{r})$ is the momentum-independent part of the gap function; $\Delta_{1,2} = \Delta_0^{e,h}$ at $T = 0$ and $H = 0$.

In the vortex state the self-consistent determination of the spatially dependent order parameter is a complex task. Since we are interested in relatively low fields, when the vortices are well separated, we solve the Eilenberger equations for an order parameter that is assumed to have a single vortex form,

$$\Delta^e(\vec{\rho},H;\theta) = \Delta_1(H)\tanh\left(\frac{\rho}{0.1\xi_0^e}\right)\frac{1+r\cos 2\theta}{\sqrt{1+r^2/2}}, \quad (11a)$$

$$\Delta^h(\vec{\rho},H) = \Delta_2(H)\tanh\left(\frac{\rho}{0.1\xi_0^h}\right). \quad (11b)$$

Here $\vec{\rho} = (\rho,\phi)$ is the two-dimensional projection of the radius vector in cylindrical coordinates, and the factor of 0.1 is introduced to approximate the shrinking of the core size in the self-consistent treatment at low temperatures (the Kramer-Pesch effect[39,40]). This single-vortex ansatz provides a qualitatively correct description of the low-field state, close to what is found by full numerical solution.[31] To account for the suppression of the bulk order parameter by the magnetic field, we determine the coefficients $\Delta_{1,2}(H)$ from the Brandt-Pesch-Tewordt approximation,[41] where in the presence of an Abrikosov vortex lattice the diagonal components of the Green's function are replaced by their averages over a vortex unit cell of the vortex lattice. This approximation is proven to give reliable results over a considerable range of magnetic fields and is incorporated into our approach.

Note that our ansatz for the order parameter becomes quantitatively inaccurate for strong interband coupling in the regime of applicability of the Ginzburg-Landau theory, since the core sizes of the two bands approach each other.[42] We verified in a fully self-consistent calculation that in the parameter range that we use the corresponding effect on the specific heat is of order 1% or less and hence can be neglected. We therefore use Eq. (11) hereafter.

To proceed we substitute Eq. (11) into Eq. (6), solve for $a(x)$ and $b(x)$, and use Eq. (8) to find the local density of states $N(\vec{\rho},H)$. To approximate the specific heat coefficient, we evaluate the spatial average of the zero-energy local density of states

$$\bar{N}(H) = \int_0^{2\pi} d\phi \int_0^R d\rho\, \rho \frac{N(\vec{\rho},H)}{\pi R^2 N_0}, \quad (12)$$

where the intervortex distance R depends on H as described by Eq. (9). The total density of states is then given as

$$\bar{N}(H)_{\rm tot} = \frac{w_e \bar{N}^e(H) + w_h \bar{N}^h(H)}{w_e + w_h}, \quad (13)$$

where $w_e/w_h = 2N_0^e/N_0^h = 2\zeta$ if we consider, for example, two electron Fermi surface sheets in the folded Brillouin zone and denote $\zeta \equiv N_0^e/N_0^h = v_F^h/v_F^e = 0.65 = \lambda_{21}/\lambda_{12}$. The specific heat Sommerfeld coefficient γ in the superconducting state is now obtained as $\frac{\gamma(H)-\gamma_0}{\gamma_n-\gamma_0} = \bar{N}(H)_{\rm tot}$. Since the vortex density is controlled by the external field, integration up to the intervortex spacing $R \sim \sqrt{\Phi_0/H}$ correctly accounts for the field effect within the single-vortex approximation. The integration thus includes not only the contribution of extended quasiparticle states to the specific heat, but also the localized quasiparticles in the core.

IV. RESULTS

To illustrate that the salient features of the vortex state DOS are captured in our approach in Fig. 3 we show the field dependence of the spatially averaged zero-energy local density of states (ZDOS) for a one-band SC with either an isotropic s-wave gap or a strongly anisotropic nodal gap ($r = 1.3$). Note that, while the field dependences in both the nodal and fully gapped cases clearly fit the anticipated power laws at low fields, $\sqrt{H}$ and H, respectively, there is a significant influence on the magnitude of the DOS caused by the size of the core, with the smaller core size yielding a smaller ZDOS. In particular, in the absence of the Kramer-Pesch effect, for the nodal case the ZDOS would exceed the normal-state value at fields far below H_{c2}, which is unphysical.

Below we consider $r = 0.9$ and 1.3 to mimic a gap with deep minima and accidental nodes, respectively. To show different types of behavior allowed within our microscopic model, we chose four sets of coupling constants, two for each value of r, as shown in Table I. In cases 1 and 3, the interband pairing λ_{12} is strong and close to the intraband parameter λ_{11}, while in cases 2 and 4 $\lambda_{12} \ll \lambda_{11},\lambda_{22}$.

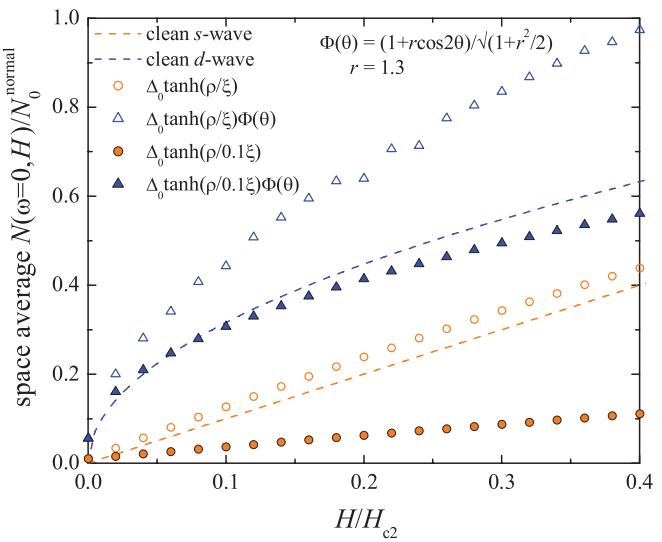

FIG. 3. (Color online) The spatially averaged ZDOS, normalized to the normal-state value $N(\omega = 0)/N_0$ for a nodeless (lower two data sets, orange) and a nodal (upper two data sets, blue) single-band superconductor. The dashed lines show the idealized linear H and $\sqrt{H}$ behavior for a clean s-wave (lower line) and d-wave (upper line) SC, respectively. The symbols are numerical results for a single-band SC with an isotropic s-wave gap (circles) and a strongly anisotropic nodal gap (triangles). Additionally we compare results that do (solid symbols) and do not (open symbols) take into account the vortex core reduction due to the Kramer-Pesch effect. Here we have ignored the field dependence of the superconducting gap, i.e., $\Delta(H) = \Delta_0$.

TABLE I. The different models for the coupling matrix and the gap anisotropy on the electron pockets considered in this work.

	λ_{11}	λ_{12}	λ_{21}	λ_{22}	r	T_c (K)	H_{c2} (T)
Case 1	0.51	0.51	0.33	0.65	0.9	31	54
Case 2	1.00	0.02	0.013	0.81	0.9	31	47
Case 3	0.51	0.51	0.34	0.64	1.3	31	54
Case 4	1.00	0.023	0.015	0.77	1.3	31	42

In Fig. 4(a) we show the self-consistently determined magnitudes of the bulk gaps in the vortex state $\Delta_{1,2}(H)$ as defined in Eqs. (10) and (11). $H_{c2} \sim 40$–50 T. In the cases 2 and 4 with only weak interband pairing, the gap on the electron Fermi surface deviates considerably from the phenomenological form $\Delta(H) = \Delta_0\sqrt{1 - H/H_{c2}}$. Figures 4(b) and 4(c) show the spatially averaged ZDOSs corresponding to each band. For $N^e(H)$ and for $r = 1.3$ the $\sqrt{H}$ behavior of the Volovik effect is clearly visible at lower fields. Comparing Fig. 4(b) to Fig. 3, we find that within the two-band model the density of states on the electron band $N^e(H)$ reaches a quasilinear behavior already at smaller fields than the corresponding density of states for the one-band case. In Fig. 3 a linear behavior is never observed, and might only be fitted over some intermediate field range for $H/H_{c2} > 0.2$, while in the multiband case $N^e(H)$ displays a clear linear behavior already for $H/H_{c2} > 0.1$.

It is tempting to interpret the low-field crossover to a quasilinear field variation as evidence for a small energy scale $\Delta_{\rm sm} \equiv \Delta_0^e(1-r)/\sqrt{1+r^2/2}$ on the electron band; this, however, seems unlikely. Provided $\Delta_{\rm sm} \ll \Delta_0^e$, the gap still increases linearly along the Fermi surface away from the nodal points above this energy scale, simply with a different slope. Then within the usual Volovik argumentation the contributions from extended states at these intermediate energies give rise to a $\sqrt{H}$ contribution even if $\Delta_{\rm sm} \lesssim E_H \ll \Delta_{\rm max}$, where $E_H \propto \sqrt{H}$ is the average Doppler shift and $\Delta_{\rm max} \equiv \Delta_0^e(1+r)/\sqrt{1+r^2/2}$ is the maximum gap. There is therefore no true linear-H behavior arising from the electron band with gap nodes. Consequently, we interpret this crossover as the consequence of the two-band behavior coupled with a gradually increasing contribution of core states which is nearly linear in field. Figure 4(c) clearly shows that the density of states on the hole band, $N^h(H)$, assumed here to be fully gapped, is always linear as a function of field, and the results for the two different coupling matrices considered here are very similar. However, as mentioned before, the slope is smaller than the one predicted for an idealized s-wave SC.

Using Eq. (13), the spatially averaged ZDOSs on the electron and the hole bands are added with different weights. Using the results presented in Figs. 4(b) and 4(c) as case 4, we investigate several cases. Since there are two electron pockets, and assuming that only one hole pocket contributes significantly to the low-energy density of states (or that a naive average over the hole pockets is sufficient), the net DOS and the field dependence of the Sommerfeld coefficient are functions only of the ratio of the densities of states on the electron and hole sheets. In the following we will study three cases that we will abbreviate by "Q," indicating the use of the quasiclassical, or Eilenberger, approach:

(1) Case Qa: we assume that only one hole pocket contributes considerably to the low-energy DOS and use the weights $w_e/w_h = 2N_0^e/N_0^h$ taken from the DFT calculation, $N_0^e/N_0^h = 0.65$ (see Ref. 37).

(2) Case Qb: We once again fix $N_0^e/N_0^h = 0.65$, but adopt a model for which the normal DOSs for all three hole pockets of $Ba_2Fe_2(As_{0.7}P_{0.3})_2$ are the same and for which all three pockets contribute equally to the low-energy DOS; hence $w_e/w_h = 2N_0^e/3N_0^h$.

(3) Case Qc: We do not hold the ratio N_0^e/N_0^h fixed, but instead calculate the weights for the electron pockets a_1 and for the hole pockets a_2 by a least-squares fit to the experimental data using the formula $\gamma^{\rm tot} = a_1\bar{N}_e(H) + a_2\bar{N}_h(H)$. If we normalize it to the presumed contribution of the superconducting fraction, $\gamma_n - \gamma_0 \approx 14$ mJ/(mol K^2), where γ_0 is the extraneous term (see below), we find $w_e/(w_e+w_h) = a_1/(\gamma_n - \gamma_0)$, $w_h/(w_e+w_h) = a_2/(\gamma_n - \gamma_0)$, and $a_1/a_2 = w_e/w_h$.

In Fig. 5 we compare the results for all three cases to the experimentally measured specific heat coefficient (pink circles). The experimental values are obtained by extrapolating the measured specific heat coefficient γ at various temperatures to $T = 0$. The upper critical field H_{c2} is taken to be 52 T (see Ref. 12). The normal-state $\gamma_n = 16$ mJ/(mol K^2)

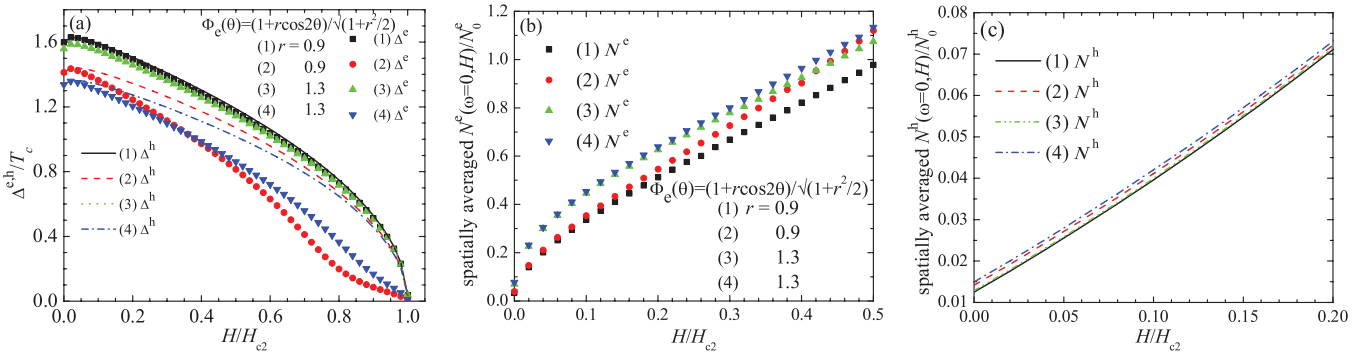

FIG. 4. (Color online) Results of quasiclassical calculations for the parameters in Table I. (a) Magnetic field dependence of the gaps in the two-band model calculated within the Pesch approximation (Refs. 41 and 43) for cases 1–4. We assume $\Delta^e(H=0) = \Delta^h(H=0)$ here. The four sets of coupling constants λ_{ij} are listed in Table I. (b) Field dependence of the space-averaged ZDOS $N^e(H)$ on the electron pocket for the four cases with anisotropic gap with angular variation $\Phi_e(\theta) = (1 + r\cos 2\theta)/\sqrt{1+r^2/2}$. (c) Field dependence of the space-averaged ZDOS $N^h(H)$ for the four cases with isotropic gap along the hole pocket.

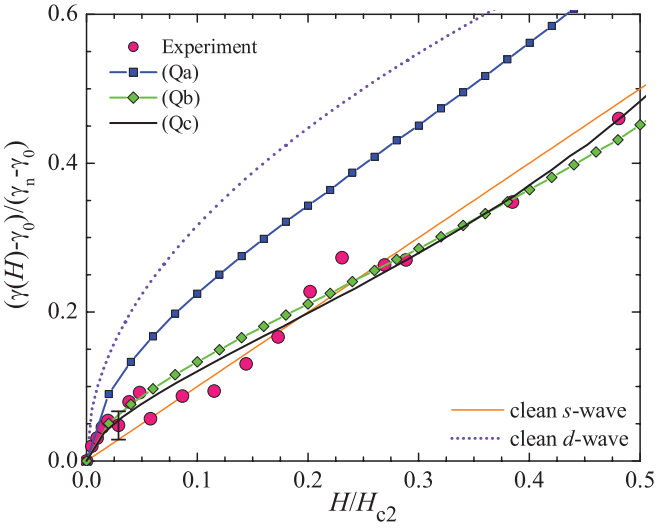

FIG. 5. (Color online) Comparison of the experimentally measured normalized specific heat coefficient (pink circles) to different theoretical results for the spatially averaged ZDOS. The dotted violet and solid orange curves are the predictions for the spatially averaged ZDOS for a clean s-wave and a d-wave SC. The blue squares (case Qa) and green diamonds (case Qb) are the differently weighted sums of $\tilde{N}^e(H)$ and $\tilde{N}^h(H)$ evaluated for case 4 of Figs. 4(b) and 4(c). The black line (no symbols) (case Qc) is obtained using the formula $\gamma^{\rm tot} = a_1\tilde{N}_e(H) + a_2\tilde{N}_h(H)$, where $a_1 = 3.2$ mJ/(mol K^2), $a_2 = 10.3$ mJ/(mol K^2) are determined with a least-squares fit to experimental data below 30 T. Note that the "d-wave" and "s-wave" curves represent simple extrapolations of the low-field $\sqrt{H}$ and H terms up to H_{c2}. The error bar shown corresponds to the absolute accuracy of the data discussed above in Fig. 1.

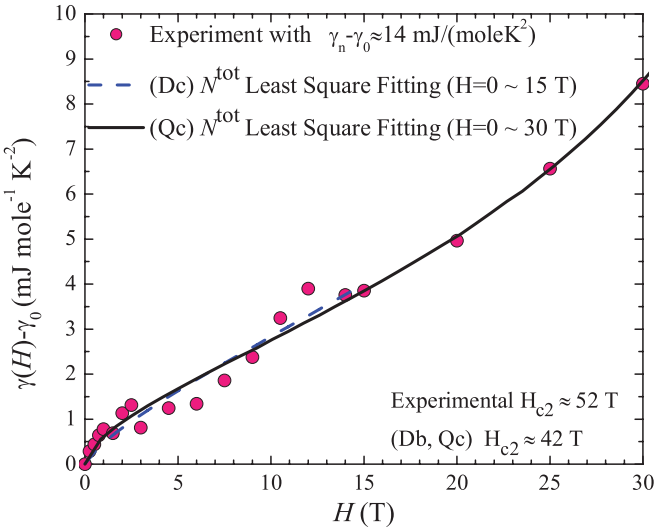

FIG. 6. (Color online) $\gamma^{\rm tot}$ plotted with experimental data in absolute units. Case Qc is the black solid line similar to that in Fig. 5. Case Dc is obtained using the formula $\gamma^{\rm tot} = a_1\tilde{N}_e(H) + a_2\tilde{N}_h(H)$, where $\tilde{N}_e(H)$ and $\tilde{N}_h(H)$ are represented by the open squares and circles in Fig. 8 and $a_1 = 1.50$ mJ/(mol K^2), $a_2 = 65.6$ mJ/(mol K^2) for case Dc are determined with a least-squares fit to the experimental data below 15 T.

can be obtained by extrapolating γ to H_{c2}. A substantial residual[13] $\gamma_0 = 1.7$ mJ/(mol K^2) in the superconducting state, presumed due to disorder, is subtracted in the plots of the field dependence from the experimental data (pink circles) to compare with our quasiclassical calculation in the clean limit (blue squares and green diamonds). Note that subtraction of the residual C/T tends to enhance the scatter in the low-T data of Fig, 2.

From Fig. 5, we see that the results derived for model Qb with three equal-mass hole pockets and two equal-mass electron pockets are in good agreement with the experimental data: both experiment and theory show a "Volovik effect" at the lowest fields and then a crossover to a linear H dependence at intermediate fields. While model Qa has the same qualitative behavior, the relative weights of hole and electron bands are apparently not consistent with the normalized experimental data, and the fit is much poorer. Compared to model Qb the least-squares fit (Qc) to the experimental data (black line) is only marginally improved, and gives $N_0^e/N_0^h = 0.47$ with two electron pockets and three hole pockets or 0.16 with two electron pockets and one hole pocket, the same order as obtained from DFT.

For completeness it is important to determine whether the experimental data can be appropriately fitted within the confines of a simple two-band Doppler-shift approach. We detail this method in the Appendix, where we show that models a and b do not give a satisfactory fit to the experiment. In contrast, model c yields a rather similar field dependence of the field-induced enhancement of the Sommerfeld coefficient for the quasiclassical and Doppler (Dc) methods, as shown in Fig. 6. At the same time the best-fit linear coefficients for model Dc, $a_1 = 1.50$ mJ/(mol K^2), $a_2 = 65.6$ mJ/(mol K^2), give the ratio of the normal-state DOSs for two electron and three hole Fermi sheets of $N_0^e/N_0^h = 3a_1/2a_2 \approx 0.03$, very different from the value of 0.65 obtained within the band structure calculations. Consequently, the quasiclassical method provides a far more satisfying fit to the data.

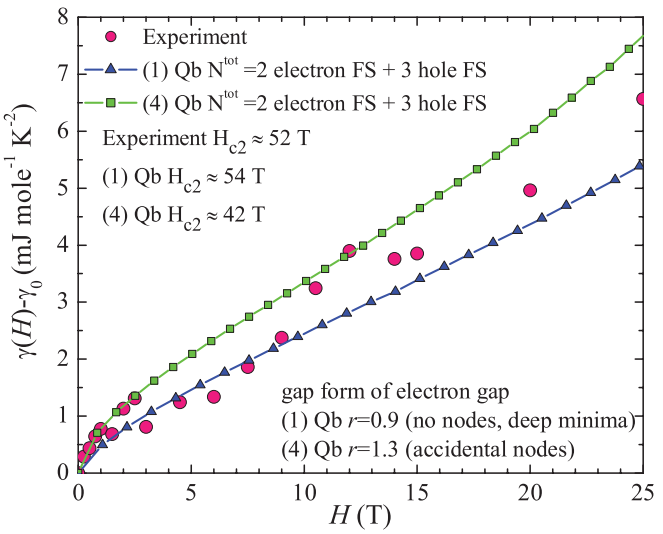

FIG. 7. (Color online) Experimentally measured specific heat coefficient (pink circles) compared to calculations with deep gap minima (case 1, $r = 0.9$, blue triangles) and accidental nodes (case 4, $r = 1.3$, green squares). In both cases the weight of electron and hole pocket contributions has been chosen in agreement with case Qb.

As is usually the case with measurements that probe the amplitude rather than the phase of the gap, it is difficult to distinguish the deep minima from the nodes. In this case we find that with our current uncertainty in the band parameters, and the scatter in the data, it is impossible to assert the nodal behavior purely from the current data. Figure 7 shows the comparison of cases 1 and 4 of Table I, corresponding to $r = 1.3$ and 0.9, i.e., with and without true nodes, with the weights of case Qb. Even though the nodal fit appears better at the lowest fields, higher-H data are in between the two cases. Therefore the conclusion about the true node comes from data from other experiments, such as the penetration depth.

V. CONCLUSIONS

Among the various families of Fe-based superconductors, $BaFe_2(As_{1-x}P_x)_2$ may be a key system for understanding the origins of superconductivity. In part this is because, alone among the materials thought to display nodes in the superconducting gap, it possesses a rather high T_c of 31 K, and hence the interplay of the pairing mechanism and Fermi surface shape and parameters in determining the gap anisotropy is under special scrutiny. The lack of an observable Volovik effect in earlier specific heat measurements was a cautionary note in an otherwise consistent array of measurements in support of gap nodes. In this paper, we have presented new experimental data at both lower and higher fields than previous measurements, and found that the initially reported linear-H behavior extends up to 35 T, but that at low fields ($H \lesssim 4$ T) more precise measurements with smaller gradations in the change of field between data points are now clearly consistent with a Volovik-type effect. The residual $T \to 0$ Sommerfeld coefficient $\gamma(T \to 0)$ is about 1.7 mJ/mol K^2, consistent with possible nanoscale disorder in the sample. The low-field sublinear dependence of the Sommerfeld coefficient is a strong indication that nodes (or deep minima) are present and provides the sought-after consistency with other probes without us having to make extreme assumptions about the ratio of masses on electron pockets to those on hole pockets, as was proposed in Ref. 13.

It is nevertheless striking that indications of nodal behavior on the same samples are so much weaker in the specific heat measurements as compared to thermal conductivity and penetration depth measurements. This is clearly indicating that the nodes are located on the pockets with smaller masses and/or longer lifetimes, as was pointed out in Ref. 13. We have attempted to put this statement on a semiquantitative basis by presenting a quasiclassical (Eilenberger) calculation of the density of states and specific heat of a two-band anisotropic $s_\pm$ superconductor. Comparison with the Doppler-shift method allowed us to argue that the quasiclassical calculation is superior for semiquantitative purposes. We find that the unusually small range of Volovik-type behavior, followed by a large range of linear-H behavior, is due to the small gap and weak nodes on the small-mass (presumably electron) sheet.[12,13] Good fits to the data are obtained for average hole and electron maximum gaps of approximately equal magnitude, in the weak-interband-coupling limit. The success of this fit should not, however, tempt one to draw definitive conclusions about the relative magnitudes of the pairing interactions. The proliferation of parameters in the theory makes it difficult to determine gap magnitudes, density of states ratios, and nodal properties with any quantitative certainty. Equally good fits can be obtained, for example, with substantially smaller full gaps than anisotropic gaps; the nodes control the low-field behavior, and the small full gap gives rise to a large linear term. What is important is that we have shown that a fit can be obtained with reasonable values of the parameters, that it can only be obtained if nodes exist on one of the Fermi sheets, and that it requires going beyond the simple Doppler-shift picture. It is our hope that the results of this calculation and fit will eventually lead to a more quantitative first-principles-based calculation.

ACKNOWLEDGMENTS

The authors are grateful to F. Ronning for useful discussions. Y. W. and P. J. H. were supported by the DOE under Grant No. DE-FG02-05ER46236, and G. R. S. and J. S. K. under Grant No. DE-FG02-86ER45268. I. V. acknowledges support from DOE Grant No. DE-FG02-08ER46492. S. G., P. H., Y. M., T. S., and I. V. are grateful to the Kavli Institute of Theoretical Physics for its support and hospitality during the research and writing of this paper.

APPENDIX: COMPARISON WITH THE DOPPLER-SHIFT METHOD

In the following we briefly discuss the basic concepts of the Doppler-shift method and compare it to the quasiclassical approximation as manifested in the formulation of the Eilenberger equations introduced in the main text. The Doppler-shifted energy due to the local supercurrent flow is $\omega - m\mathbf{v}_F \cdot \mathbf{v}_s(\mathbf{r})$, where

$$m\mathbf{v}_F^{e,h} \cdot \mathbf{v}_s(\mathbf{r}) = \frac{\hbar}{2|\mathbf{r}|}\mathbf{v}_F^{e,h}(\theta) \cdot \mathbf{e}_\phi = \frac{\hbar v_F^{e,h}}{2|\mathbf{r}|}\sin(\theta - \phi) = \frac{\Delta_0^{e,h}}{2\tilde{\rho}^{e,h}}\sin(\theta - \phi). \tag{A1}$$

Here, we assume $\Delta^e(T = 0, H = 0) = \Delta^h(T = 0, H = 0) = \Delta_0^{e,h}$ and use $\tilde{\rho}^{e,h} = |\mathbf{r}|/\xi_0^{e,h}$. Therefore the normalized local DOS is

$$N(\omega, \mathbf{r}) = \int_0^{2\pi} \frac{d\theta}{2\pi} \mathrm{Re}\left\{\frac{|\omega - m\mathbf{v}_F \cdot \mathbf{v}_s(\mathbf{r})|}{\sqrt{(\omega - m\mathbf{v}_F \cdot \mathbf{v}_s(\mathbf{r}))^2 - |\Delta(\theta)|^2}}\right\}, \tag{A2}$$

and thus the normalized spatially averaged DOS is

$$\bar{N}(H) = \int_0^{\tilde{R}} \frac{d\tilde{\rho}\,\tilde{\rho}}{\pi\tilde{R}^2} \int_0^{2\pi} d\phi \int_0^{2\pi} \frac{d\theta}{2\pi} \times \mathrm{Re}\left\{\frac{|\omega - \Delta_0 \sin(\theta - \phi)/(2\tilde{\rho})|}{\sqrt{[\omega - \Delta_0 \sin(\theta - \phi)/(2\tilde{\rho})]^2 - |\Delta(\theta)|^2}}\right\}. \tag{A3}$$

Here we have introduced the normalized vortex cell radius $\tilde{R} = R/\xi_0^e$ for the electron bands and R/ξ_0^h for the hole bands, respectively. Since the Doppler-shift method does not capture core-state contributions it underestimates the slope

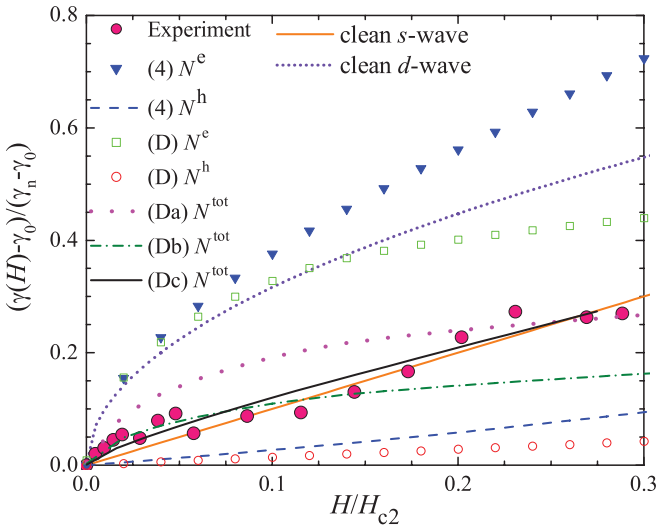

FIG. 8. (Color online) Normalized specific heat coefficient determined within the quasiclassical approach (blue triangles and blue dashed curve) and within the Doppler-shift method (open squares and circles). Total normalized specific heat coefficients obtained within the Doppler-shift method are shown by magenta dotted line, olive dash-dotted line, and black solid line for cases Da, Db, and Dc, corresponding to Qa, Qb, and Qc, respectively. The dotted violet and solid orange curves are the power laws predicted for the spatially averaged ZDOSs of an idealized s-wave and a d-wave SC. Pink circles show the experimentally determined normalized specific heat coefficient.

of the magnetic field dependence of the zero-energy DOS of an s-wave SC. Since the core region gives only negligible contributions to the total DOS, one can in principle avoid the divergence of the Doppler-shift energy as $\tilde{\rho} \to 0$ by cutting out the complete core region with a lower limit ξ_0 for the radial integration. Here we have included the core region when integrating over the vortex unit cell. To model $\Delta(\theta)$ we use a similar function as given by Eq. (11), but without explicitly modeling the core structure:

$$\Delta^e(\vec{\rho};\theta) = \Delta_1(H=0)\frac{1+r\cos 2\theta}{\sqrt{1+r^2/2}}, \tag{A4a}$$

$$\Delta^h(\vec{\rho}) = \Delta_2(H=0), \tag{A4b}$$

and we use the self-consistently calculated $\Delta_{1,2}(H=0)$ in case 4 of the quasiclassical calculation in which the anisotropy factor $r = 1.3$ for the gap along the electron Fermi surface sheet and the ratio of the normal DOSs at the Fermi energy is taken as $N_0^e/N_0^h = 0.65$. In Fig. 8 we show the results obtained within the Doppler-shift approach and compare them to case 4 of the quasiclassical method. Again we also show predictions for idealized clean s- and d-wave SCs. We conclude that the Doppler-shift method and the quasiclassical method give comparable results at the lowest fields but start to deviate as soon as the field increases. One reason might be that with increasing field and decreasing intervortex distance the core states that are not correctly accounted for within the Doppler-shift method but captured within the quasiclassical approach become increasingly more important. However, due to the limitations of the single-vortex approximation the overlapping of vortices is not correctly reproduced and the DOS is overestimated (in Fig. 8 the blue triangles rise too fast).

In Fig. 6 we compare the least-squares fit by the Doppler-shift method (blue dashed curve) to the least-squares fit by the quasiclassical method (the black line similar to that in Fig. 5) and experimental data (pink circles). The linear coefficients for case Dc are $a_1 = 1.50$ mJ/(mol K^2) and $a_2 = 65.6$ mJ/(mol K^2). Compared to the linear coefficients for case Qc [$a_1 = 3.2$ mJ/(mol K^2) and $a_2 = 10.3$ mJ/(mol K^2)), they give a nonphysical ratio of the normal DOSs at the Fermi energy if we consider two electron Fermi sheets and three hole Fermi sheets. To see this point, let us consider the equation

$$\begin{aligned} C_{e,h}(T,H) &= \frac{1}{2}\int_{-\infty}^{+\infty} d\omega \frac{\omega^2 \tilde{N}_{e,h}(H,\omega)}{T^2\cosh(\omega/2T)} \\ &\approx A\tilde{N}_{e,h}(H,\omega)T \qquad (\text{as} T \to 0) \\ &\Rightarrow \gamma_{e,h} \approx A\tilde{N}_{e,h}(H,0) \equiv AN_0^{e,h}\bar{N}_{e,h}(H,0). \end{aligned} \tag{A5}$$

Here A is a numeric constant and we write $\tilde{N}_{e,h}(H,0) \equiv N_0^{e,h}\bar{N}_{e,h}(H,0)$, where $\bar{N}_{e,h}(H,0)$ is the ZDOS calculated by the Green's function method as defined in Eq. (12). Denote the number of Fermi sheets included in the summation as $n_{\rm FS}$ and define $n_{\rm FS}^e AN_0^e = a_1$ and $n_{\rm FS}^h AN_0^h = a_2$ (equivalent to $w_e = n_{\rm FS}^e N_0^e$ and $w_h = n_{\rm FS}^h N_0^h$). Therefore $\gamma^{\rm tot} = a_1\bar{N}_e(H) + a_2\bar{N}_h(H)$. Note that $\bar{N}_{e,h}(H)$ are dimensionless and $a_{1,2}$ are in units of mJ/(mol K^2). Optimized parameters $a_{1,2}$ for the least-squares fit (Dc) to the experimental data below 15 T are $a_1 = 1.50$ and $a_2 = 65.6$. This leads to our estimates in the main text of $a_1/a_2 = (n_{\rm FS}^e AN_0^e)/(n_{\rm FS}^h AN_0^h) = (2N_0^e)/(3N_0^h)$ and $N_0^e/N_0^h = 0.03$, and to our conclusion that the Doppler-shift method does not provide a satisfying physical explanation for our specific heat experiment.

[1] Y. Kamihara, T. Watanabe, M. Hirano, and H. Hosono, J. Am. Chem. Soc. **130**, 3296 (2008).
[2] F. Hsu *et al.*, Proc. Natl. Acad. Sci. **105**, 14262 (2008).
[3] H. Wen, Annu. Rev. Condens. Matter Phys. **2**, 121 (2011).
[4] G. Stewart, e-print arXiv:1106.1618, Rev. Mod. Phys. (to be published).
[5] A. Kemper, T. Maier, S. Graser, H. Cheng, P. Hirschfeld, and D. Scalapino, New J. Phys. **12**, 073030 (2010).
[6] P. Hirschfeld, M. Korshunov, and I. Mazin, Rep. Prog. Phys. **74**, 124508 (2011).
[7] S. Kasahara, T. Shibauchi, K. Hashimoto, K. Ikada, S. Tonegawa, R. Okazaki, H. Shishido, H. Ikeda, H. Takeya, K. Hirata, T. Terashima, and Y. Matsuda, Phys. Rev. B **81**, 184519 (2010).
[8] S. Jiang, H. Xing, G. Xuan, C. Wang, Z. Ren, C. Feng, J. Dai, Z. Xu, and G. Cao, J. Phys.: Condens. Matter **21**, 382203 (2009).

[9]H. Shishido, A. F. Bangura, A. I. Coldea, S. Tonegawa, K. Hashimoto, S. Kasahara, P. M. C. Rourke, H. Ikeda, T. Terashima, R. Settai, Y. Ōnuki, D. Vignolles, C. Proust, B. Vignolle, A. McCollam, Y. Matsuda, T. Shibauchi, and A. Carrington, Phys. Rev. Lett. **104**, 057008 (2010).

[10]K. Hashimoto, M. Yamashita, S. Kasahara, Y. Senshu, N. Nakata, S. Tonegawa, K. Ikada, A. Serafin, A. Carrington, T. Terashima, H. Ikeda, T. Shibauchi, and Y. Matsuda, Phys. Rev. B **81**, 220501 (2010).

[11]Y. Nakai, T. Iye, S. Kitagawa, K. Ishida, S. Kasahara, T. Shibauchi, Y. Matsuda, and T. Terashima, Phys. Rev. B **81**, 020503 (2010).

[12]M. Yamashita, Y. Senshu, T. Shibauchi, S. Kasahara, K. Hashimoto, D. Watanabe, H. Ikeda, T. Terashima, I. Vekhter, A. B. Vorontsov, and Y. Matsuda, Phys. Rev. B **84**, 060507 (2011).

[13]J. S. Kim, P. J. Hirschfeld, G. R. Stewart, S. Kasahara, T. Shibauchi, T. Terashima, and Y. Matsuda, Phys. Rev. B **81**, 214507 (2010).

[14]In contrast to $BaFe_2(As_{1-x}P_x)_2$, recent high-field measurements on underdoped ($x = 0.045$) and overdoped ($x = 0.103$) $BaFe_{2-x}Co_xAs_2$ have found that the specific heat coefficient varies approximately as $H^{0.7}$ all the way up to $H_{c2}(0)$ [J. S. Kim, G. R. Stewart, K. Gofryk, F. Ronning, and A. S. Sefat (unpublished)].

[15]Y. Bang, Phys. Rev. Lett. **104**, 217001 (2010).

[16]V. G. Kogan and J. Schmalian, Phys. Rev. B **83**, 054515 (2011).

[17]G. Stewart, Rev. Sci. Instrum. **54**, 1 (1983); B. Andraka, G. Fraunberger, J. S. Kim, C. Quitmann, and G. R. Stewart, Phys. Rev. B **39**, 6420 (1989).

[18]J. Kim, E. Kim, and G. Stewart, J. Phys.: Condens. Matter **21**, 252201 (2009).

[19]G. Eilenberger, Z. Phys. **214**, 195 (1968).

[20]A. I. Larkin and Y. N. Ovchinnikov, Sov. Phys. JETP **28**, 1200 (1969).

[21]J. Serene and D. Rainer, Phys. Rep. **101**, 221 (1983).

[22]G. E. Volovik, JETP Lett. **58**, 469 (1993).

[23]K. A. Moler, D. L. Sisson, J. S. Urbach, M. R. Beasley, A. Kapitulnik, D. J. Baar, R. Liang, and W. N. Hardy, Phys. Rev. B **55**, 3954 (1997).

[24]Y. Wang, B. Revaz, A. Erb, and A. Junod, Phys. Rev. B **63**, 094508 (2001).

[25]M. Ichioka, N. Hayashi, N. Enomoto, and K. Machida, Phys. Rev. B **53**, 15316 (1996).

[26]N. Schopohl and K. Maki, Phys. Rev. B **52**, 490 (1995).

[27]M. Ichioka, N. Hayashi, and K. Machida, Phys. Rev. B **55**, 6565 (1997).

[28]M. Ichioka, A. Hasegawa, and K. Machida, Phys. Rev. B **59**, 184 (1999).

[29]M. Franz and Z. Tešanović, Phys. Rev. Lett. **84**, 554 (2000).

[30]I. Vekhter and A. Vorontsov, Physica B **403**, 958 (2008).

[31]T. Dahm, S. Graser, C. Iniotakis, and N. Schopohl, Phys. Rev. B **66**, 144515 (2002).

[32]N. Schopohl, e-print arXiv:cond-mat/9804064v1 [cond-mat.supr-con].

[33]Note that our notation of g, f, and $\bar{f}$ differs from the one used in Ref. 32. Under the transformation $g \to -i\pi g$, $f \to \pi f$, and $\bar{f} \to -\pi \bar{f}$, the notation in Ref. 32 passes into our notation.

[34]K. Suzuki, H. Usui, and K. Kuroki, J. Phys. Soc. Jpn. **80**, 013710 (2011).

[35]T. Shimojima *et al.*, Science **332**, 564 (2011).

[36]V. Mishra, G. Boyd, S. Graser, T. Maier, P. J. Hirschfeld, and D. J. Scalapino, Phys. Rev. B **79**, 094512 (2009).

[37]V. Mishra, S. Graser, and P. J. Hirschfeld, Phys. Rev. B **84**, 014524 (2011).

[38]T. Yoshida, I. Nishi, S. Ideta, A. Fujimori, M. Kubota, K. Ono, S. Kasahara, T. Shibauchi, T. Terashima, Y. Matsuda, H. Ikeda, and R. Arita, Phys. Rev. Lett. **106**, 117001 (2011).

[39]L. Kramer and W. Pesch, Z. Phys. **269**, 59 (1974).

[40]W. Pesch and L. Kramer, J. Low Temp. Phys. **15**, 367 (1974).

[41]U. Brandt, W. Pesch, and L. Tewordt, Z. Phys. **201**, 209 (1967); W. Pesch, Z. Phys. B **21**, 263 (1975).

[42]M. E. Zhitomirsky and V.-H. Dao, Phys. Rev. B **69**, 054508 (2004).

[43]P. Klimesch and W. Pesch, J. Low Temp. Phys. **32**, 869 (1978).